RESEARCH PAPER
Contrib. Sci. & Tech Eng, 2024, 1(4)
Homepage: https://cste.journals.umz.ac.ir/
DOI: 10.22080/cste.2025.28235.1006

Numerical Investigation of Suction Parameters for Boundary Layer Control on an Airfoil with Gurney Flap

Korosh Hassanzadeh [1], Alireza. Hasibi [2], Mohsen Pourfallah [3], Bahram Jafari [4]*, Khashayar Hosseinzadeh [5]

[1] *Department of Mechanical Engineering, Mazandaran University of Science and Technology, Babol, Iran.*

[2] *Department of Mechanical Engineering, Babol Noshirvani University of Technology, Babol, Iran.*

[3] *Department of Mechanical Engineering, Tennessee Tech University, Cookeville, TN, USA*

[4] *Faculty of Engineering Modern Technologies, Amol University of Special Modern Technologies (AUSMT), Amol, Iran.*

[5] *Department of Mechanical Engineering, University of Mazandaran, Babolsar, Iran.*

Article Info
Received 21 December 2024
Accepted 12 January 2025
Available online 07 March 2025

Keywords:
NACA 0012 Airfoil;
Gurney Flap;
Vertical Suction;
Suction Angel;
Drag Force.

Abstract:
The present study numerically investigated the impact of suction and its related parameters, including dimensionless suction velocity, suction angle, and suction length, on controlling the flow over a NACA 0012 airfoil with a Gurney flap. The height of the gurney flap is 2% of the cord. The Reynolds number of the flow is 2.1×10^6, which is entirely turbulent. Turbulent flow has been analyzed using the Reynolds stress model (RSM). The suction on the airfoil is modeled as uniform and normal (vertical suction), and the length of the suction area is 3% of the chord length (CHL) (3cm). The suction jet is designed at two angles of 60 and 90 degrees. The results indicate that with the rise of the suction dimensionless velocity, the drag coefficient (C_D) decreases. The maximum ratio of forward to backward dimensionless velocity due to suction is one, occurring at a position 2.5% of the chord length (CHL). This indicates that for optimal performance, the jet suction on the airfoil should be positioned at 2.5% of the CHL. The results of this study contribute to the development of a novel method for boundary layer (BL) control, aiming to optimize drag force on airfoils for improved flow management.

***Corresponding Author:** mpourfall42@tntech.edu, B.jafari@ausmt.ac.ir

Supplementary information: Supplementary information for this article is available at https://cste.journals.umz.ac.ir/

Please cite this paper as: Ghessisin, S. M., Behforouz, B., Fathi, F., & Hosseini, S. J. (2025). Improving the Seismic Performance of Precast Post-Tensioned RC Shear Walls by applying FRP Sheets. Contributions of Science and Technology for Engineering, 1(4), 58-72. doi:10.22080/cste.2025.28235.1006.

1. Introduction

Flow control is a highly significant subject in fluid mechanics and has been studied by many researchers for more than fifty years. A key objective of flow control is to manage separation and enhance aerodynamic coefficients (A.Cs), including drag and lift. Fluid mechanics experts are particularly interested in studying the impact of the BL and its regional separation on the drag and lift coefficients (CL), especially when analyzing the hydrodynamic characteristics of hydrofoils. BL control strategies, also known as the flow separation control method, can increase or decrease the CD. These strategies are ubiquitous and several years old. They improve the CD and CL by affecting the BL separation point. The suction air strategy for boundary layer (BL) control has recently emerged as a novel method. This approach can delay or eliminate the separation point, significantly impacting aerodynamic coefficients (A.Cs).

Ravindran [1] conducted a numerical analysis to examine the impact of unstable suction and blowing on oil airfoils. A tangential jet introduces unstable suction and blows at the leading edge of the tile airfoil. The findings suggest that unstable suction and blowing can effectively be employed as a method of separation control to produce lift on airfoils. In an experimental study, Li et al. [2] analyze the pressure distribution on the surface and the profiles of the wake of a NACA0012 airfoil. The purpose was to calculate the CL, CD, and pitching moment for different configurations. The data demonstrates that including a Gurney flap significantly enhanced the maximum CL, elevating it from 1.37 to 1.74. Nevertheless, there was an increase in CD at a CL that ranged from low to moderate. The boundary layer (BL) profile measurements were also performed using a set of total pressure probes arranged in a rake configuration positioned at the 90% chord region on the suction side. Huang et al. [3] conducted an experiment where they positioned a jet with a width equal to 2.5% of the CHL over

*ISSN **3060-6578***

the upper surface of a NACA0012 airfoil. This setup aimed to simulate the effects of suction and blowing control under certain conditions: the Reynolds number (Re) is 5×10^5, and the angle of attack was 18 degrees. The essential parameters of suction and blowing, including their positions, amplitudes, and angles, were carefully considered. The practical implementation of extensive numerical simulations provides a valuable foundation for future investigations into multi-jet control systems. To examine the influence of synthetic jets (SJs) on the separation of turbulent flow over an airfoil, You et al. [4] implemented a large-eddy simulation. They evaluated the effectiveness of slot jets (SJs) in managing flow separation. Their experiment involved airflow over a NACA 0015 airfoil at a Reynolds number (Re) of 896,000, calculated using the airfoil's chord length (CHL) and the velocity of the surrounding air. To produce oscillatory slot jets (SJs), a narrow slit extending the full length of the airfoil was connected to an internal cavity. Large-eddy simulations confirmed that synthetic-jet actuation effectively delayed flow separation and significantly improved the coefficient of lift (CL). Kim et al. [5] performed a computational analysis to investigate the aerodynamic properties of a NACA23012 airfoil with SJs, focusing on separation control. The numerical findings showed that resizing separating vortices might significantly enhance stall features and control surface efficiency. The highest amount of lift was achieved when the point of separation aligned with the position of the SJ, and the frequency was around 1, measured in non-dimensional units. Furthermore, the degree of separation control was directly related to the maximum velocity of the SJ. Liu et al. [6] developed an innovative suction-blowing joint management system to reduce the airfoil's drag coefficient (CD). This method involved blowing air at the trailing edge and suction at the airfoil's leading edge. The numerical results demonstrated that this suction-blowing control strategy reduces CD more effectively than suction alone without blowing. These numerical analyses establish a valuable foundation of knowledge for future investigations into the design of 3-D wing suction-blowing control. Genç et al. [7] evaluated the effectiveness of transition and turbulence models in predicting low Reynolds number flows with laminar separation bubbles, which are typically difficult to forecast using RANS-based CFD methods. Furthermore, they examined mitigating laminar separation bubbles on a solitary airfoil by implementing blowing and suction techniques. The results indicated that the separation bubble is not entirely destroyed in the blowing and suction scenarios but rather reduced or shifted further downstream. Abdullah et al. [8] experimented to investigate how continuous, regular suction applied to the upper surface of a wing affects aerodynamic forces. They explored the effects of the placement of suction slot passages and the mass flow rate of the extracted air. The wing prototype utilizing the NACA 0015 profile has been designed to provide a controlled suction effect on the upper surface of the wing through the use of four slot channels. The findings demonstrated that the consistent application of normal suction substantially improved the CL-to-CD force ratio. Furthermore, it was noted that this ratio increased more significantly with the intensity of the suction. Yagiz et al. [9] evaluated the feasibility of diminishing the shock wave and consequently decreasing the wave drag during Supersonic flight by implementing flow control mechanisms, such as a single jet actuator and 2-D contour bump, and combining both control devices known as hybrid control. The results showed that optimizing the design parameters of both passive and active control devices led to a 3.94% reduction in the total drag coefficient (CD) and a 5.03% increase in the coefficient of lift (CL). Shi et al. [10] examined a numerical method for implementing hybrid laminar flow control (HLFC) on a suction slot with a width ranging from 0.5 mm to 7 mm. The results indicate that this transition prototype can accurately predict transitional conditions with suction control. For this study, a carefully designed laminar airfoil was selected. The single-hole simulation results suggest that increasing the suction coefficient and positioning the slot nearer to the trailing edge can effectively delay the transition and reduce drag. Zhang et al. [11] performed a computational study on the suction control of flow separation of a NACA0012 airfoil. The study considered a Re of 104 and angle of attack (α) values of 2°, 4°, 6°, and 8°, as well as a Re of 105 and α of 4°. The study examines the inhibitory effects of suction, considering many characteristics like suction coefficient, position, angle, hole diameter, and porosity. The fluctuations in energy use and CL-CD ratio during the control process are utilized to assess the effectiveness of the control measures. Zhao et al. [12] conducted a computational investigation on the effect of SJ control on the unstable dynamic stall of a rotor airfoil. A system incorporating a moving-embedded grid and a solver based on the URANS equations, along with the k-ω Shear Stress Transport (SST) turbulence model, has been developed to precisely predict the complex flow patterns around an oscillating airfoil with jet control. The simulation results show that the effectiveness of jet control can be improved by optimizing the momentum coefficient and jet angle, particularly when the jet is positioned near the separation point of the rotor airfoil. Ma et al. [13] utilized a water tunnel experiment and computational methods to examine the effects of suction flow management on the flow condition and aerodynamic force of the wing at a low Reynolds number. Additional research was carried out to investigate the effects of suction flow rate and suction position on transition, laminar separation, and the aerodynamic efficiency of the wing. The findings indicated that suction may effectively regulate laminar separation and transition. The most optimal control effect was achieved when the suction slots were positioned within the inside of the separation bubble and near the point of separation. Kamari et al. [14] utilized both blowing and suction techniques to manipulate the flow field by extensively breaching the BL on the airfoils' upper surface. Both techniques were utilized on the Selig–Donovan 7003 (SD7003) airfoil at a Re of 60,000. A genetic algorithm (GA) was employed as an optimization tool to determine the optimal parameters for blowing/suction. The results demonstrated that implementing active flow management techniques led to a decrease in the area of flow separation, resulting in enhanced A.Cs. It was discovered that suction proved to be a more efficient control mechanism compared

to blowing. Kamranpay et al. [15] conducted a numerical investigation of the NACA 0012 airfoil. The study involved analyzing airflow and Mach number 0.5 and assessing the coefficient of lift (CL), coefficient of drag (CD), and pressure coefficients at various angles of attack. The results show that, due to its symmetrical design, the airfoil has a CL of zero at an angle of attack of zero. However, its CD is approximately 0.01384, and the pressure coefficient is around -0.483. Karasu et al. [16] performed experiments and numerical analyses on various airfoils to study and understand the effect of camber ratio on flow characteristics over their surfaces. For the NACA 4412 airfoil, the transition position was identified using instantaneous voltage output data, while surface oil flow visualization studies were conducted for the NACA 2415 airfoil. The research provided data on turbulent kinetic energy and the ratio u/U∞ for the NACA 4415 airfoil. The experimental results demonstrated that thickness and camber ratio changes significantly influenced flow phenomena, including boundary layer separation and the formation and development of laminar separation bubbles. Fatahian et al. [17] performed a computational investigation to ascertain the ideal hinge position for enhancing the aerodynamic efficiency of the NACA 0012 flapping airfoil. The experiments were performed at a Re of 5×105 (Ma = 0.021) using 2-D incompressible unstable RANS computations. The purpose was to find the appropriate position for the hinge. The findings indicate that the hinge's position significantly impacts the airfoil's aerodynamic performance. Specifically, applying suction perpendicular to the flow led to an increase in the coefficient of lift (CL) and a decrease in the coefficient of drag (CD). Akbari [18] utilized a numerical solution approach to examine the aerodynamic characteristics of the NACA 6212 airfoil at different attack angles ranging from -20 to +20 degrees. Their results indicated that, overall, raising the angle of attack increases both the CD and the magnitude of the pressure coefficient. For positive assault angles, the CL rises as the attack angles grow. However, the CL declines for negative attack angles as the attack angles increase. Fatahian et al. [19] conducted a CFD study to examine the combined impact of suction and cavity on regulating separation of the flow on the NACA 0012 airfoil. The fluid flow is considered to be incompressible, 2-D, and turbulent. The results indicate a 30% rise in the CL and a 40% decrease in the CD at an angle of attack of 14° while employing simultaneous cavity and suction. Using the flow control approach enhances the CL-to-CD ratio, resulting in a rise in the stall angle from 14° to 22°. Kumar et al. [20] performed a numerical investigation on the impact of various airfoil-slat Settings for the NACA 2415 airfoil. They used the FVM, k-ω-SST, and k-kl-ω turbulence models for the simulations. The highest CL for a solitary aerodynamic slat was achieved at $\alpha = 22°$, with a value of 2.22. For a double aerodynamic slat, the maximum CL was obtained at $\alpha = 26°$, with a value of 2.33 at a Re of 2×10^5. It was noticed that the CL increased by 72% with a single-slat setting compared to the airfoil without slats. Zhu et al. [21] utilized numerical simulations to examine the aerodynamic properties of a 3-D Co-Flow Jet (CFJ) wing equipped with basic high-lift devices throughout the low-speed landing and takeoff phases. The detailed examination focuses on the impacts of three critical elements of the CFJ wing: swept angle, jet momentum, and angle of attack. The findings indicated that utilizing the CFJ approach on a wing equipped with a basic high-lift device can provide more CL, decrease CD, and expand the stall margin while minimizing energy consumption because of the super-circulation phenomenon. Açıkel et al. [22] constructed and customized the tubular configuration to fit the NACA0012 airfoil shape. The tubercle wing was simulated using numerical modeling in ANSYS FLUENT. The Transition SST turbulence and k-ω SST models in numerical simulation investigated the tubercle wing performance. The findings indicated that the aerodynamic efficiency of the wing was enhanced when the wing's leading edge was equipped with sinusoidal protrusions, also referred to as tubercle structure. Mishra et al. [23] performed a computational study to examine the effect of flow management on NACA0021 airfoils by adding a leading-edge tubercle. The aim was to enhance the efficiency of wind turbines operating at a transitional Re range. The experiment involves conducting simulations on both the original and modified airfoil. These simulations are conducted at a Re of 120,000, using a delayed detached eddy simulation model based on the kT-kL-ω approach. The modified airfoil exhibits a progressive stall characteristic, in contrast to the sharp stall behavior of the base airfoil. To enhance the tubercle setting, the test examines two modified airfoils with varying mixtures of wavelength and amplitude. Ma et al. [24] compared two flow control strategies, which used both blowing and suction, on the pitching airfoil. The study utilized the URANS approach. The S809 airfoil was chosen as the basis because of its suitable stall feature for investigating stall control or separation flow. The results suggested that the C-CFJ is appropriate for no-stall and mild-stall situations, whereas the R-CFJ is more appropriate for deep-stall situations. Regarding suppressing the dynamic stall, leading-edge suction provides more stability than leading-edge blowing. Useful articles on this subject can be read as follows [25-28].

The current study uses numerical analysis to examine the effects of suction and its associated factors, such as dimensionless suction velocity, suction angle, and suction length, on managing the flow over a NACA 0012 airfoil with a Gurney flap. The gurney flap is 2% of the cord's height. The airfoil's suction is modelled as usual and uniform (vertical suction), with a suction area length of 3% of the chord length. There are two angles of 60 and 90 degrees in the design of the suction jet. The RSM has been used to analyze turbulent flow.

2. Mathematical Model and Formulation

The Navier–Stokes equations offer a comprehensive mathematical model for fluid dynamics. However, their complexity makes obtaining analytical solutions in their complete form impractical. Consequently, numerical methods, facilitated by computer simulations, are the most effective approach for solving these equations.

2.1. Continuity and Momentum Equations for Turbulent Flow

For compressible flow, we have

$$\frac{\partial}{\partial x_i}(\overline{\rho\, u_i}) + \frac{\partial}{\partial x_i}(\overline{\rho'\, u_i'}) = 0 \quad (1)$$

Since the incompressible flow rate is $\rho' = 0$, the above equation will be as follows:

$$\frac{\partial \bar{u}_i}{\partial x_i} = 0 \quad (2)$$

The general momentum equation for turbulent flow has been defined as follows:

$$\rho\left[\frac{\partial \bar{u}_i}{\partial t} + \bar{u}_j\frac{\partial \bar{u}_i}{\partial x_j}\right] = \bar{B}_i - \frac{\partial \bar{p}}{\partial x_i} + \frac{\partial}{\partial x_j}\left[\mu\frac{\partial \bar{u}_i}{\partial x_j} - \rho\overline{u_i'u_j'}\right] \quad (3)$$

The sole distinction between the aforementioned momentum equation and the momentum equation using simultaneous quantities is adding the last term on the right side of the equation, $\rho\overline{u_i'u_j'}$. This term is referred to as turbulence stress or Reynolds stress.

2.2. Turbulence Model

Given the flow velocity, air is treated as an incompressible fluid with constant physical properties. This study focuses on steady, two-dimensional flow. The flow is assumed to be fully turbulent, with a Mach number less than 0.3 in all cases. As the flow is incompressible, the numerical simulation does not include the energy equation. The RNG k-ε turbulence model is employed, with turbulent kinetic energy k and its dissipation rate ε determined using the following equations:

$$\frac{\partial}{\partial t}(\rho k) + \frac{\partial}{\partial x_i}(\rho k u_i) = \frac{\partial}{\partial x_j}\left(\alpha_k \mu_{\varepsilon f}\frac{\partial k}{\partial x_j}\right) + \mathrm{G}_k + \mathrm{G}_b + \rho\varepsilon - \mathrm{Y}_M + \mathrm{S}_k \quad (4)$$

$$\frac{\partial}{\partial t}(\rho \varepsilon) + \frac{\partial}{\partial x_i}(\rho \varepsilon u_i) = \frac{\partial}{\partial x_j}\left(\alpha_\varepsilon \mu_{\varepsilon f}\frac{\partial \varepsilon}{\partial x_j}\right) + \mathrm{C}_{1\varepsilon}\frac{\varepsilon}{k}(\mathrm{G}_k + \mathrm{C}_{3\varepsilon}\mathrm{G}_b) - \mathrm{C}_{2\varepsilon}\rho\frac{\varepsilon^2}{k} - \mathrm{R}_\varepsilon + \mathrm{S}_\varepsilon \quad (5)$$

G_k indicates the production of kinetic energy of turbulence due to the average velocity gradient. G_b indicates the production of kinetic energy because of the buoyancy force. α_k and α_ε are the reciprocal of the Prandtl number for k and ε, respectively.

3. Geometry and Mesh

This study examines the NACA 0012 airfoil, which has a chord length (CHL) of 1 meter. The airfoil is modeled using a C-shaped mesh network. To create a regular mesh, the solution domain around the airfoil is considered blocked, extending 12.5 times the chord length in all directions from the airfoil's edges. Due to the complex flow and high vorticity intensity around the Gurney flap, an excellent mesh layer with a cell width of 0.5 mm has been implemented. The Gurney flap, installed at the airfoil's trailing edge at a 90-degree angle and extending 2% of the CHL (2 cm), is depicted in Figure 1, which shows the airfoil geometry and meshing.

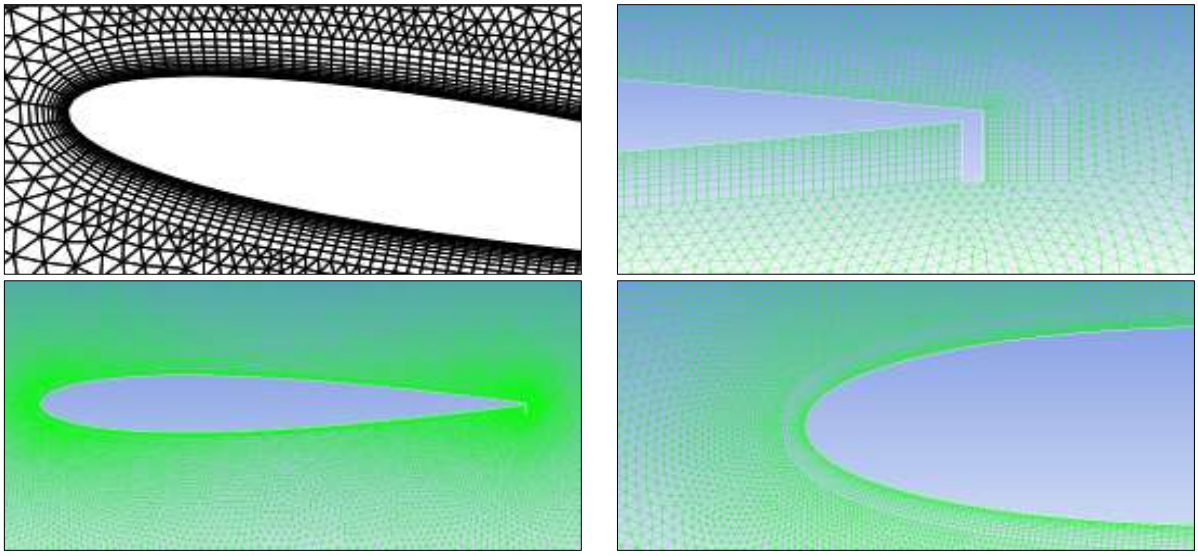

Figure 1. Airfoil geometry and meshing

4. Validation

The RNG k-ε model was validated by Li et al. [2] and Krishnaswamy et al. [29] studies to investigate the Gurney flap at high Reynolds numbers. The governing equations of the flow field are thoroughly turbulent for all simulations. For all cases, the Ma number is less than 0.3, the flow is incompressible, and therefore, the energy equation is not used for numerical simulations. To check the Gurney flap, the networks produced in ICEM have been confirmed to have at least 200,000 nodes.

The airfoil boundary is defined as a solid wall with no-slip conditions, while the inlet is assigned as the inlet velocity and the outlet as the outlet pressure. The density-based density uses airflow and a Ma number less than 0.3. Therefore, the liquid has a constant density of 1.225 kg/m^3 and a dynamic viscosity of 1.7894 x $10^{(-5)}$ kg/m-s. According to experimental research, the value of the Reynolds number based on the length of the airfoil and the inlet velocity is 2.1×10^6. Using this Reynolds number, the inlet flow velocity is 30.67. The convergence coefficient for

all solution variables is set at 0.8. The residual convergence criterion of the solution is set at 0.00001.

Since laboratory data for lift coefficient are available in the article, validation has been done for different angles of attack from 0 to 18 degrees. Figure 2 illustrates a comparison of C_L in different attack angles.

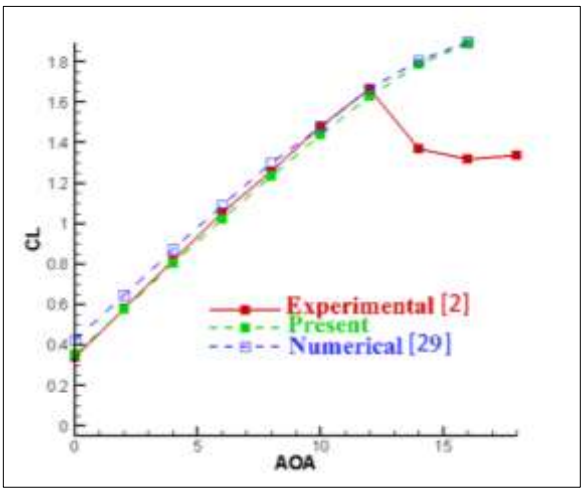

Figure 2. Comparison of CL in different attack angles

5. Result and Discussion

5.1. The impact of the Gurney flap on lift coefficient

The flow field around a flat airfoil and a Gurney flap with a height of 2 cm placed at the trailing edge can be observed in Figure 2. The flow field is displayed using the flow lines and creating a color pattern of the pressure contours on those lines. The counterclockwise vortices created by the Gurney flap move downstream, creating a stagnation point outside the airfoil's trailing edge. The counterclockwise vortices downstream of the Gurney flap create a low-pressure area and reduce the average pressure gradient close to the escape edge. Reducing the thickness of the BL prevents the separation of the BL on the airfoil's upper surface or postpones it. Also, these vortices increase the velocity on the airfoil's upper surface and, as a result, increase the suction on the upper face of the airfoil. On the other hand, the velocity upstream of the gurney flap has decreased, which leads to a rise in the pressure on the lower surface of the airfoil. A rise in suction on the upper face and a rise in pressure on the lower face simultaneously increases the rotation of the flow around the airfoil and, finally, increases the C_L. Figure 3 shows the flow lines on simple airfoil and airfoil with a 2% Gurney flap.

5.2. The Impact of Suction on A.Cs

The length and height of the flap are considered to be 2% of the CHL. The Re of the flow is 2.1×10^6, which is entirely turbulent. Turbulent flow has been analyzed using the Reynolds stress model. The suction on the airfoil is modeled as uniform and normal (vertical suction), and the length of the suction area is 3% of the CHL (3 cm). According to previous studies, the suction jet is located at a distance of 10% and 25% of the CHL from the attack edge. Two suction velocities are considered: one at 0.5 times and the other at 1 times the free-stream velocity. The suction jet is set at two angles: 60 degrees and 90 degrees. Initially, it will be evaluated with a dimensionless suction velocity of 0.5 across various modes. Assessments with a dimensionless suction velocity of 1 will follow this. Finally, the results will be compared. Figure 4 illustrates the suction at different positions and angles relative to the airfoil.

5.2.1.Effect of Dimensionless Suction Velocity of 0.5 on A.Cs

5.2.1.1. Suction at Angles of 90 and 60 Degrees at 0.1 Chord Length

Using the suction dimensionless velocity of 0.5 at two different angles at the location of 0.1 CHL, it is concluded that there is no significant effect on the A.Cs at low attack angles. The effects were investigated for attack angles of 10 to 18 degrees. In suction with an angle of 90 degrees, fewer vortices than in suction with an angle of 60 degrees can be seen at the end of the airfoil in the flow line diagram. This subject indicates a lower pressure and a higher flow velocity on the airfoil's upper face at the end edge; as a result, the combination of these two factors will increase the C_L and decrease the C_D. Figures 5 and 6 illustrate the velocity and pressure contours with a dimensionless suction velocity of 0.5 and a suction angle of 60 and 90 degrees at 0.1 CHL, respectively.

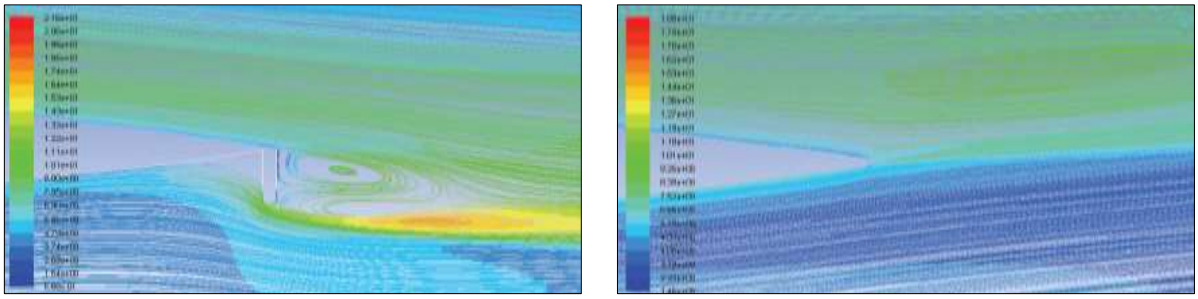

Figure 3. Flow lines on simple airfoil and airfoil with 2% Gurney flap

Homepage: https://cste.journals.umz.ac.ir/
DOI: 10.22080/cste.2025.28235.1006

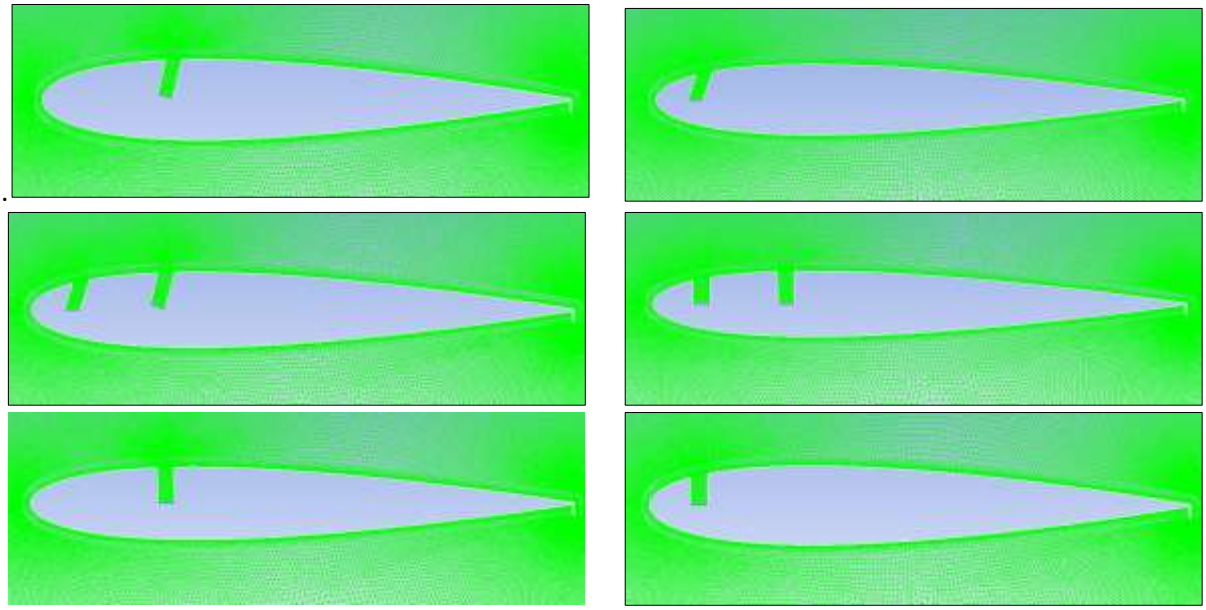

Figure 4. Suction in different positions and different angles in the airfoil

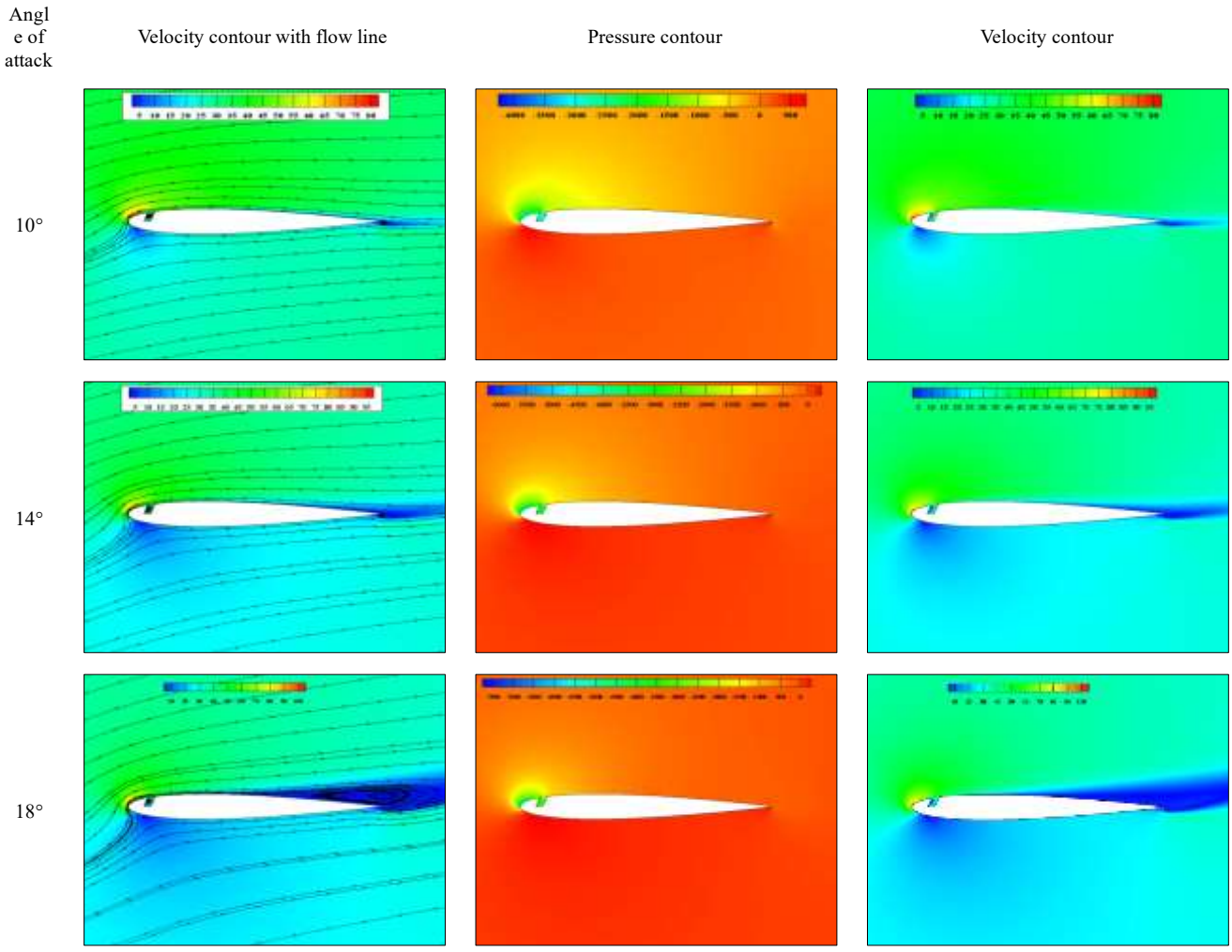

Figure 5. Velocity and pressure contours with a dimensionless suction velocity of 0.5 and a suction angle of 60 degrees at 0.1 CHL

*ISSN **3060-6578***

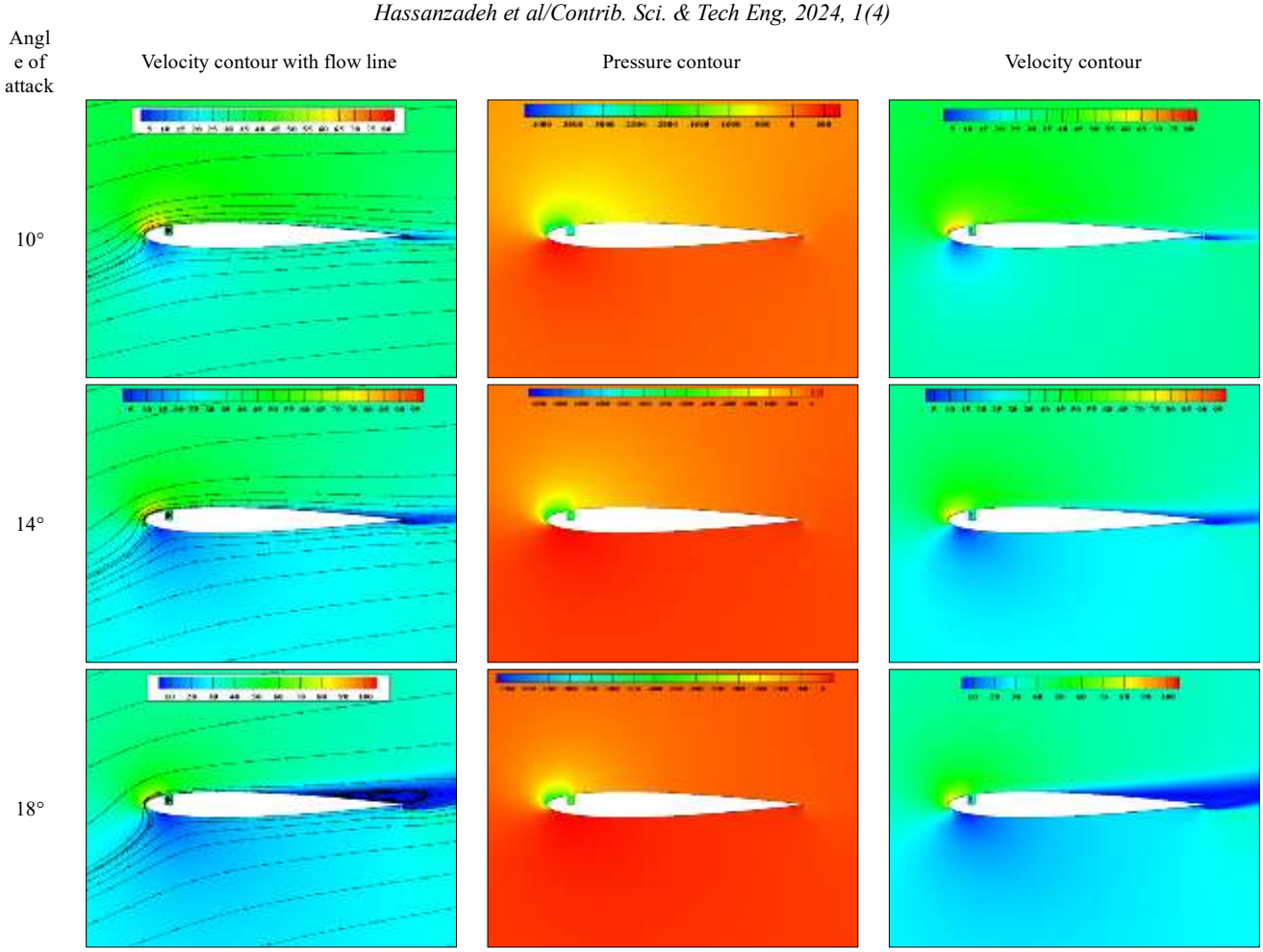

Figure 6. Velocity and pressure contours with a dimensionless suction velocity of 0.5 and a suction angle of 90 degrees at 0.1 CHL

5.2.1.2 Suction at an Angle of Attack of 90 and 60 Degrees at 0.25 Chord Length

Using a dimensionless suction velocity of 0.5 at two different angles at the location of 0.25 CHL, as in the condition of 0.1 CHL at an angle of 90 degrees, it achieved a better performance in improving the A.Cs. When comparing suction positions at 0.1 CHL and 0.25 CHL, the results show that positioning the suction at 0.25 CHL yields a higher coefficient of lift (CL). This is because the boundary layer (BL) thickens as the suction is moved closer to the end of the airfoil. As the BL thickens, the pressure on the airfoil upper surface increases, and the fluid velocity decreases, which can lead to a reduction in lift force and an increase in drag. Therefore, suction can reduce the thickness of the BL and eliminate flow separation. In the following, the velocity contour, flow line, and pressure contour are shown at the angles of attack of 10, 14, and 18 degrees. Figures 7 and 8 illustrate the velocity and pressure contours with a dimensionless suction velocity of 0.5 and a suction angle of 60 and 90 degrees at 0.25 CHL, respectively.

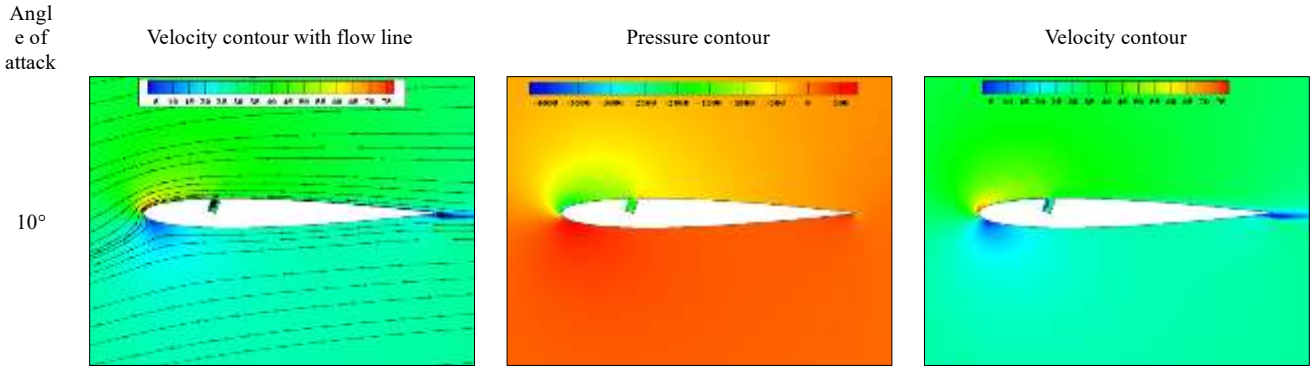

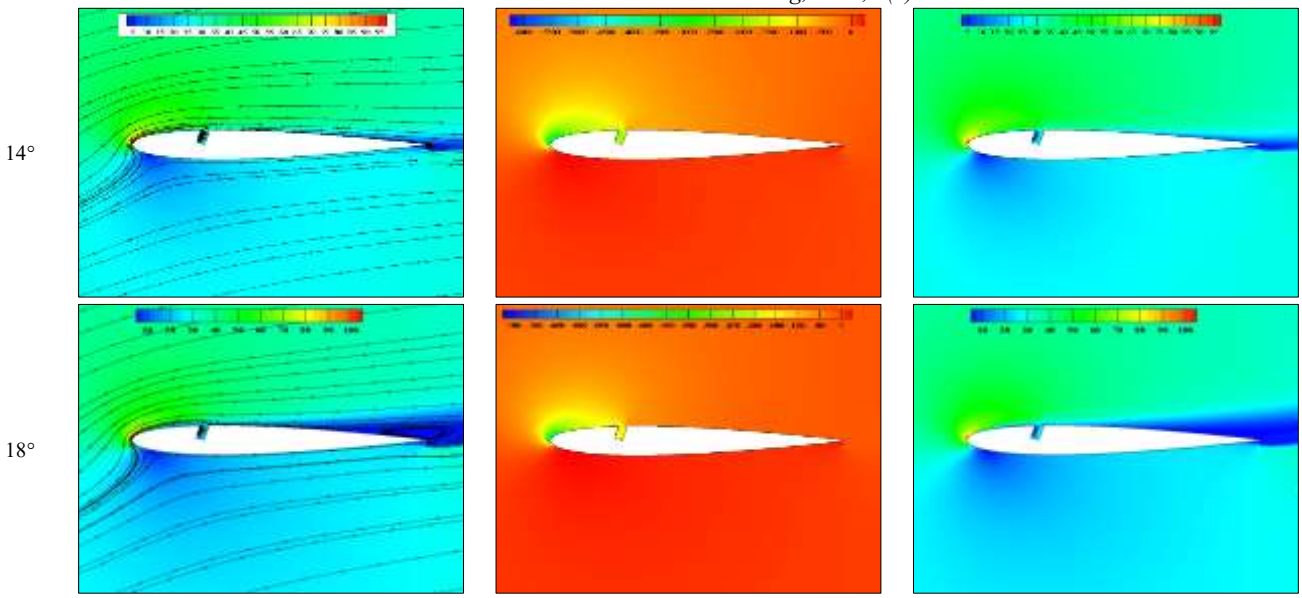

Figure 7. Velocity and pressure contours with a dimensionless suction velocity of 0.5 and a suction angle of 60 degrees at 0.25 CHL

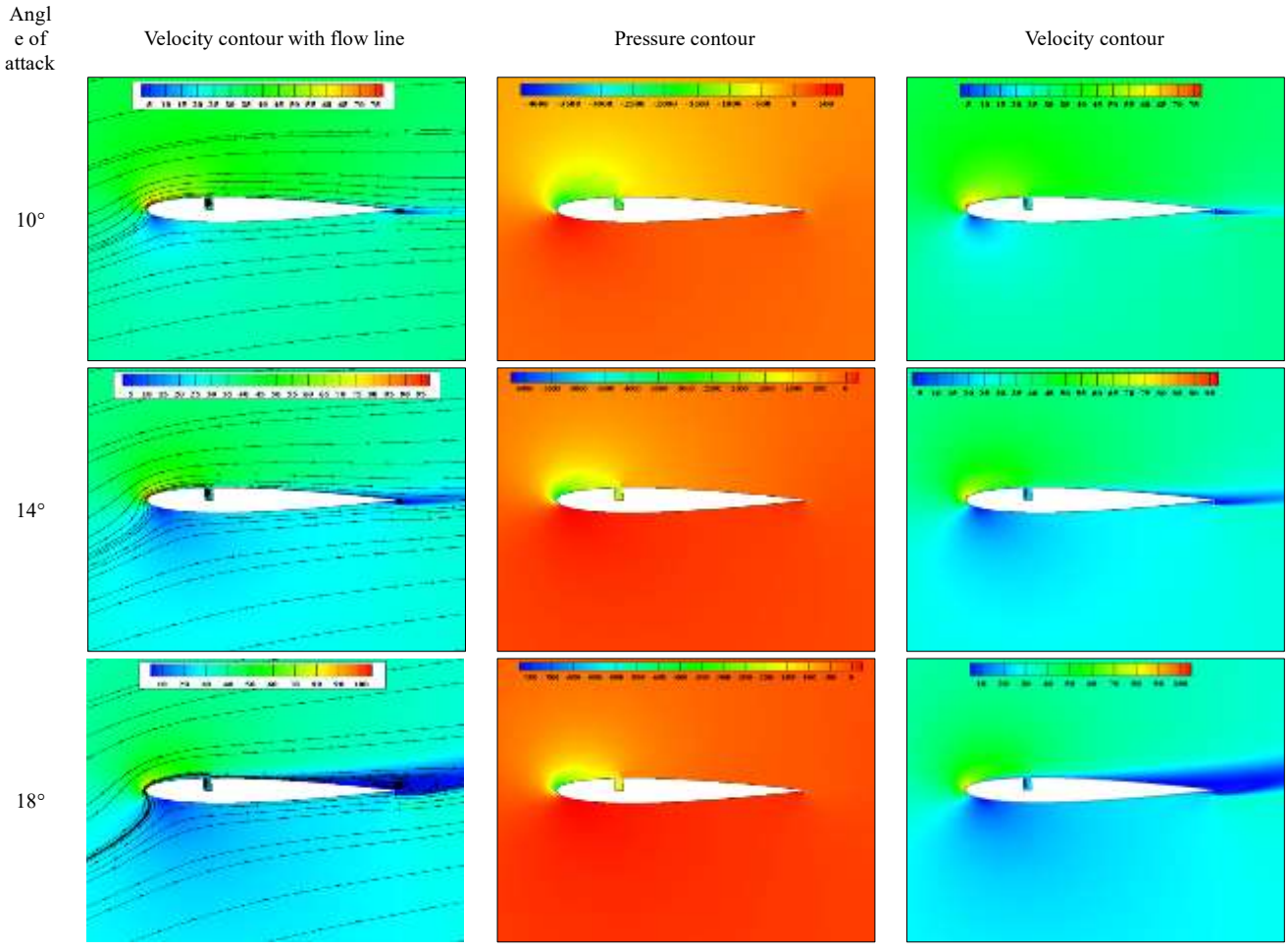

Figure 8. Velocity and pressure contours with a dimensionless suction velocity of 0.5 and a suction angle of 90 degrees at 0.25 CHL

5.2.1.3 Suction at the Angle of Attack of 90 and 60 Degrees in two Positions of 0.1 and 0.25 Chord Length

Using two suctions in one airfoil improves the A.Cs because when the primary BL is being formed, the suction at 0.1 CHL causes the loss or reduction of the thickness of this BL. As the flow continues to the end edge of the airfoil, the BL begins to grow again, the fluid velocity near the wall decreases, and the pressure on the upper surface of the airfoil begins to increase, which causes the loss of the second suction at the position of 0.25 CHL. The new BL will be formed after the first suction, so practically, it is shown that up to 0.25 CHL of the BL cannot cause changes in the A.Cs, and it will eliminate a large part of the reduction

of the C_L and cause the flow separation to be removed. Observe the contours for the two suction configurations on the airfoil: fewer vortices are formed near the trailing edge compared to the airfoil with a single suction configuration. The different contours for this mode are presented below. Figures 9 and 10 display the velocity and pressure contours for a dimensionless suction velocity of 0.5, with suction angles of 60 and 90 degrees at 0.1 and 0.25 CHL, respectively.

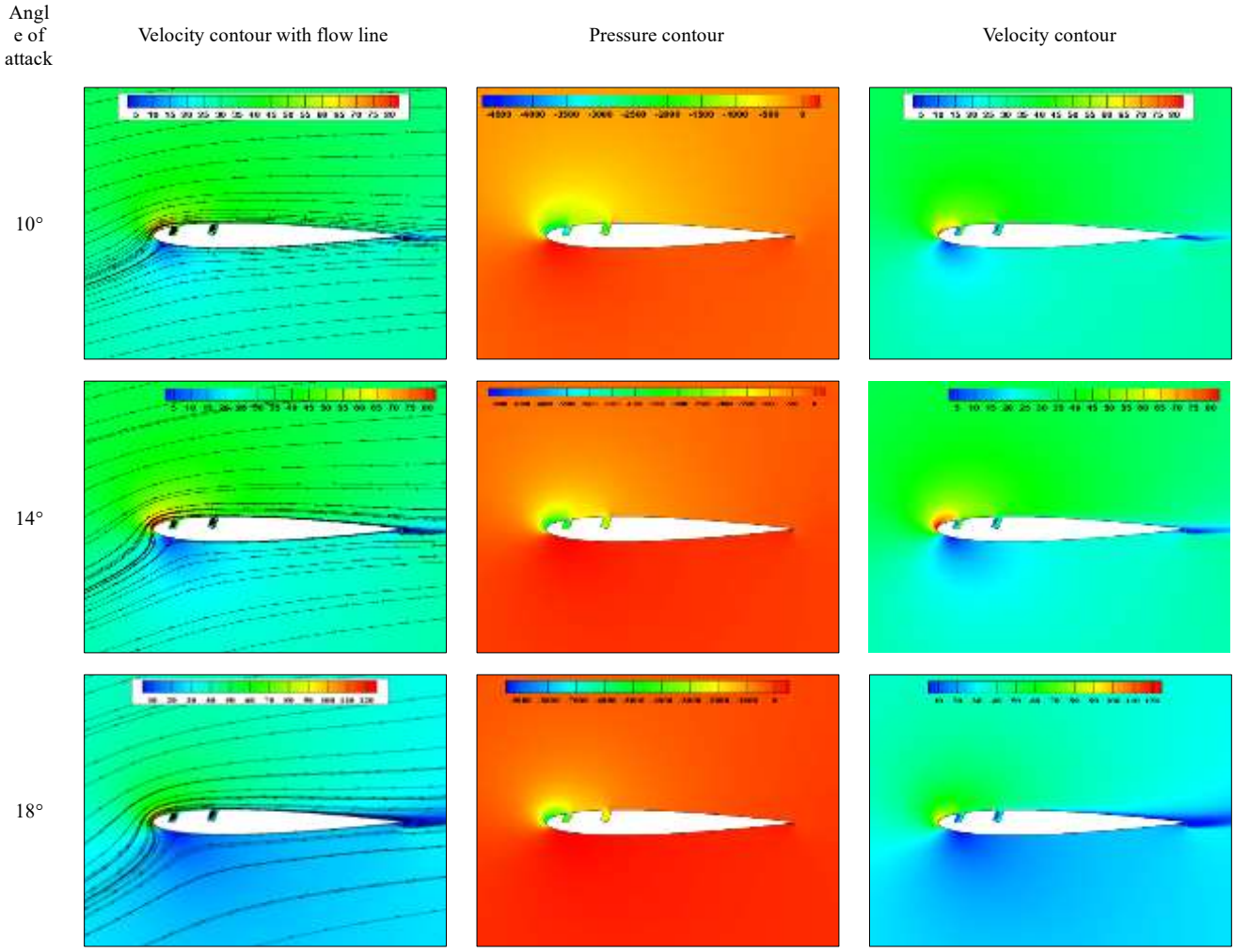

Figure 9. Velocity and pressure contours with dimensionless suction velocity of 0.5 and a suction angle of 60 degrees at 0.1 and 0.25 CHL

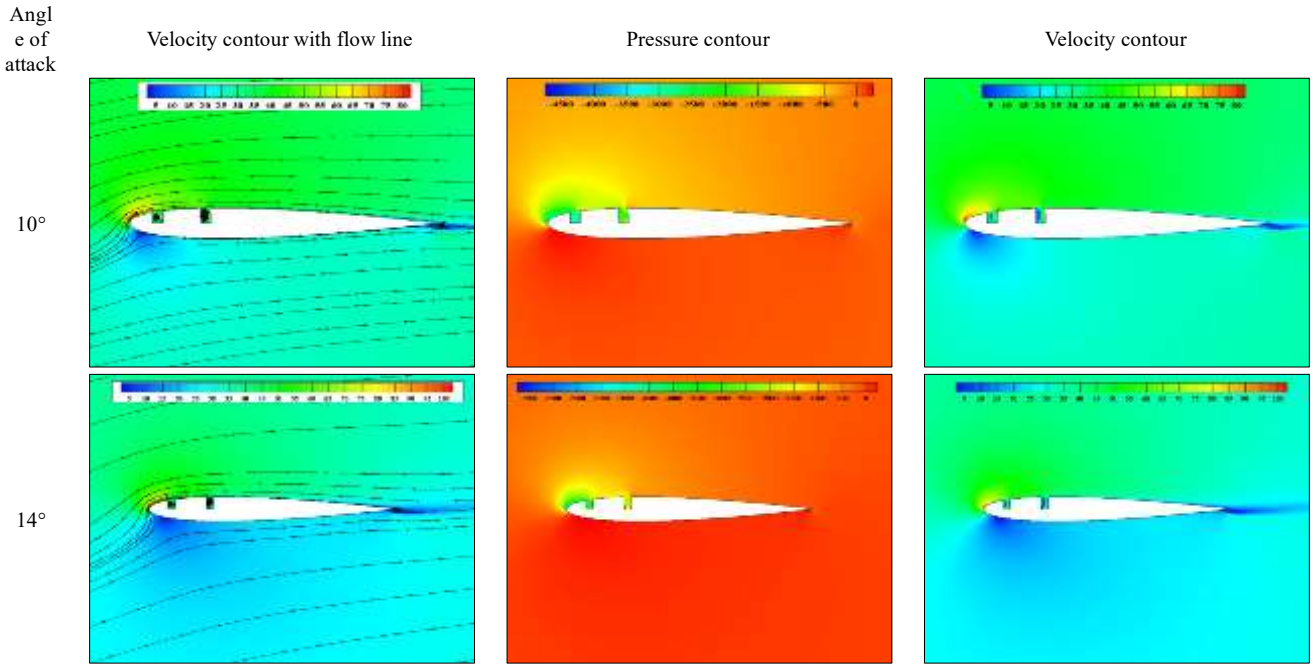

18°

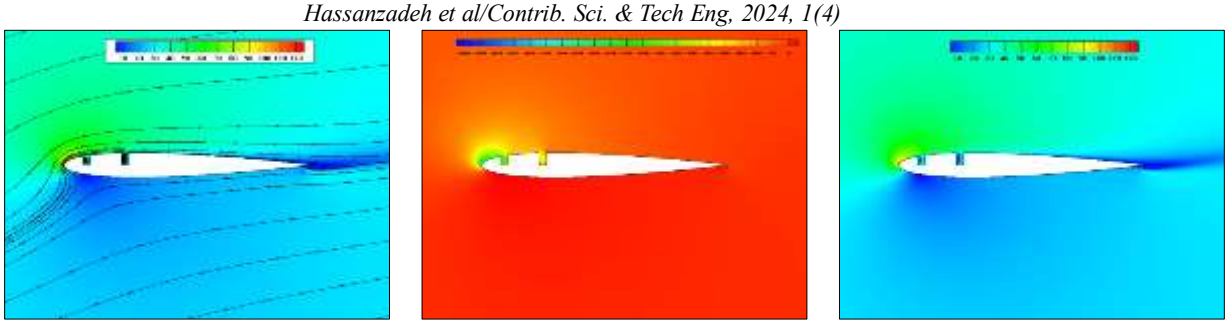

Figure 10. Velocity and pressure contours with a dimensionless suction velocity of 0.5 and a suction angle of 90 degrees at 0.1 and 0.25 CHL

5.2.2.Results in the dimensionless velocity of 0.5

The results show that the best outcomes are obtained in the airfoil with a suction of 90 degrees and a position of 0.25 CHL. Of course, this result is valid only for one suction in the airfoil; if the number of suctions in the airfoil reaches more than one number, the A.Cs will improve. The lift and C_D values show that the C_D reaches negative for two suctions in the airfoil, which shows the enhancement of A.Cs is better in the case of two suctions. Now, if two modes with different suction positions are used, the numbers obtained for the C_L show that better results are reached for the position of 0.25 CHL. For a better understanding, Figure 11 has drawn the C_L and C_D graph for attack angles of 10 to 18 degrees in suction position modes of 0.1 and 0.25 and suction angles of 60 and 90 degrees. Tables 1 and 2 depict the C_L and C_D values at a suction dimensionless velocity of 0.5 with the suction angle of 60 and 90 degrees, respectively.

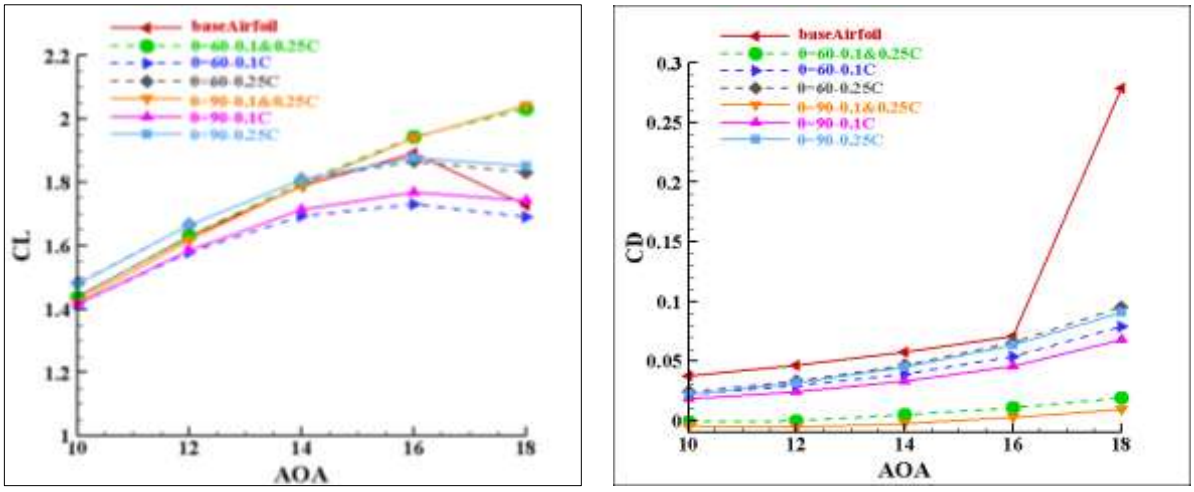

Figure 11. C_L and C_D s at different attack angles at 0.5 dimensionless velocity

Table 1. C_L and C_D values at a suction dimensionless velocity of 0.5 with a suction angle of 60 degrees

angle of attack	Suction Angle = 60 Suction position = 0.1 CHL		Suction Angle = 60 Suction position = 0.25 CHL		Suction Angle = 60 Suction position = 0.1 and 0.25 CHL	
	C_L	C_D	C_L	C_D	C_L	C_D
10°	1.1454	0.0216	1.4807	0.024	1.4361	-0.000974
12°	1.5796	0.0290	1.6639	0.0333	1.63	0.0000676
14°	1.6934	0.0392	1.8078	0.0465	1.7989	0.0046
16°	1.731	0.0537	1.8658	0.0659	1.9416	0.0107
18°	1.691	0.0790	1.8299	0.0953	2.0323	0.0192

Table 2. C_L and C_D values at a suction dimensionless velocity of 0.5 with a suction angle of 90 degrees

angle of attack	Suction Angle = 90 Suction position = 0.1 CHL		Suction Angle = 90 Suction position = 0.25 CHL		Suction Angle = 90 Suction position = 0.1 and 0.25 CHL	
	C_L	C_D	C_L	C_D	C_L	C_D
10°	1.4152	0.0181	1.4798	0.0223	1.421754	-0.00491
12°	1.5841	0.0245	1.6642	0.0315	1.615013	-0.00509
14°	1.714	0.0333	1.8086	0.0452	1.7907	-0.00242
16°	1.7676	0.0457	1.8782	0.0634	1.9405	0.00239

18°	1.7416	0.0677	1.8525	0.0911	2.0439	0.00938

5.2.3.Effect of Dimensionless Suction Velocity of 1 on A.Cs

5.2.3.1. Suction at 60° angle at 0.1 and 0.25 Chord Length and Two Suction Positions

Using suction dimensionless velocity one at two different angles at the location of 0.1 CHL, it is concluded that there is no significant effect on the A.Cs at low attack angles. It has been investigated for attack angles of 10 to 18 degrees. In suction with an angle of 90 degrees, fewer vortices than in suction with an angle of 60 degrees can be seen at the end of the airfoil in the flow line diagram, which indicates a lower pressure and a higher flow velocity on the upper surface of the airfoil at the end edge, as a result of the combination of these two the factor will increase the C_L and decrease the C_D. In the dimensionless velocity of suction 1, because the amount of suction of the flow is equal to the velocity of the flow input, compared to the dimensionless velocity of 0.5, it disturbs the BL and improves A.Cs. The contours of velocity and pressure are shown in Figures 12 and 13 at two angles of 60 and 90 degrees, respectively.

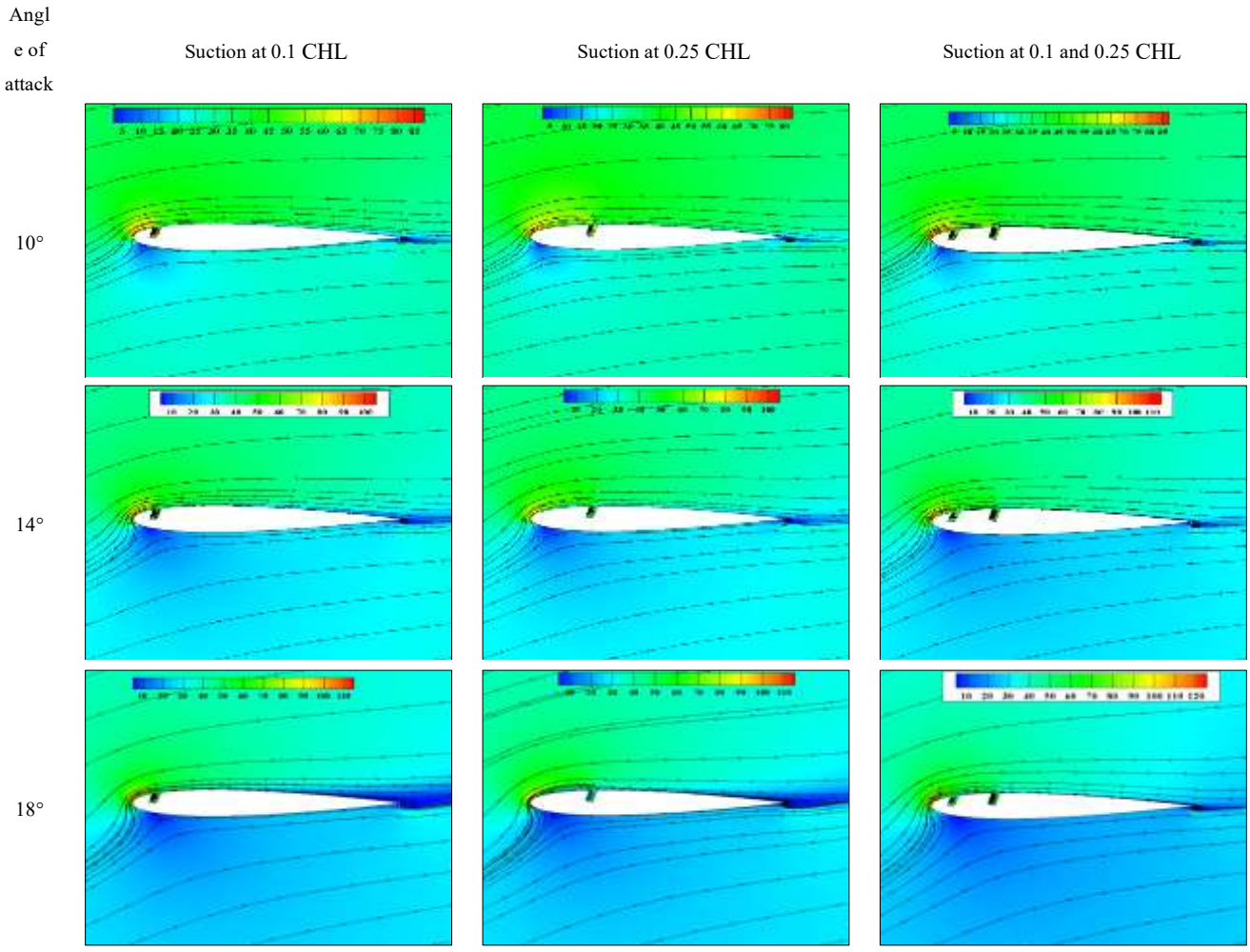

Figure 12. Velocity contours with a dimensionless velocity of suction 1 with a suction angle of 60 degrees at 0.1 and 0.25 CHL

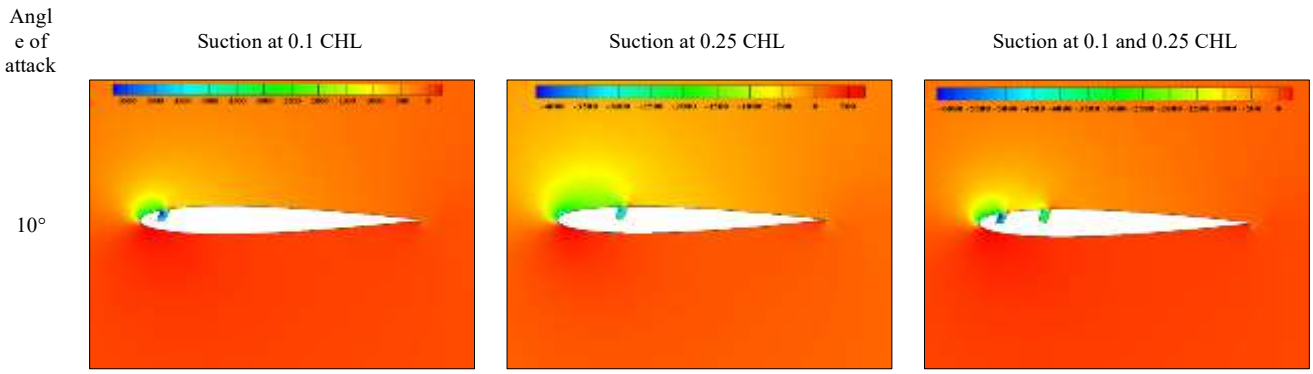

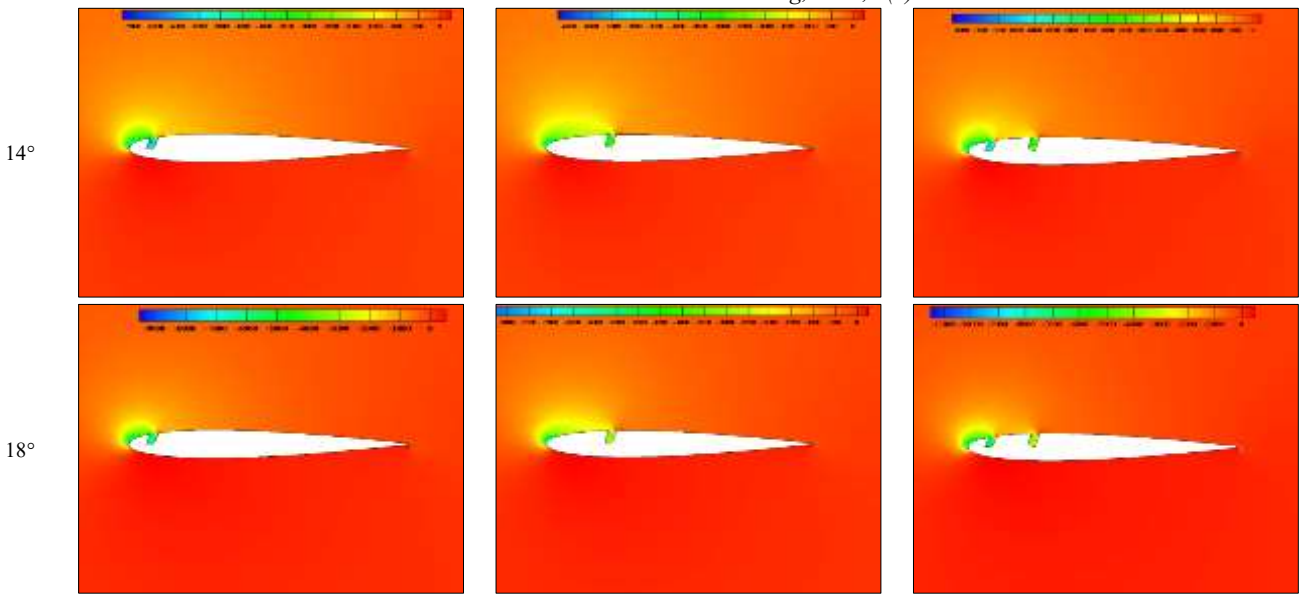

Figure 13. Pressure contours with a dimensionless velocity of suction 1 with a suction angle of 60 degrees at 0.1 and 0.25 CHL

5.2.3.1. Suction at 90° Angle at 0.1 and 0.25 Chord Length and two Suction Positions

When examining the 90-degree suction at the dimensionless suction velocity of 1, better A.Cs are obtained over the dimensionless velocity of 0.5 because when the suction velocity is higher, the separation will be lost entirely, and the thickness of the BL will be at its minimum value. In the following the velocity and pressure contours are first shown in Figures 14 and 15, which are 90 degrees, respectively.

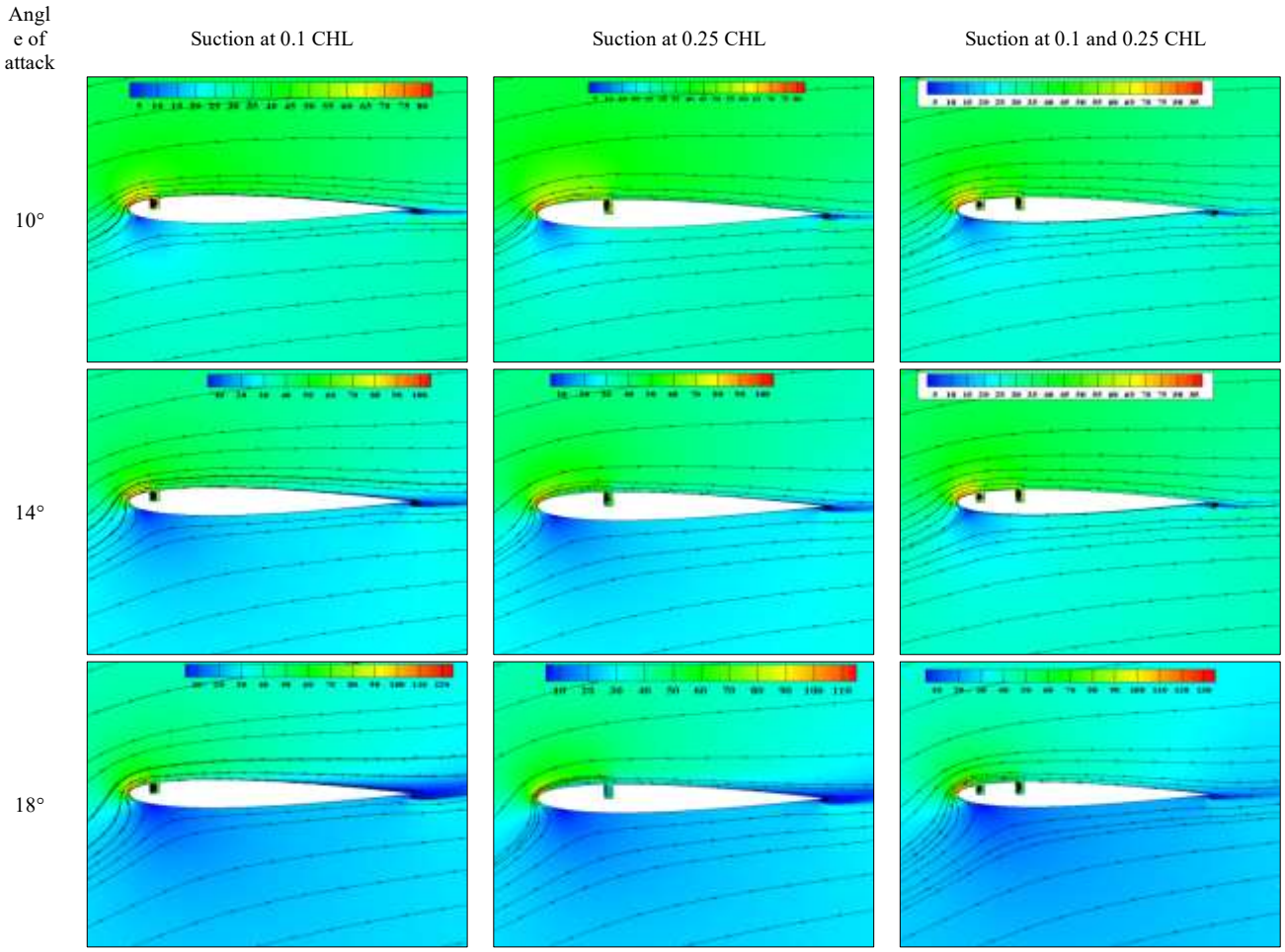

Figure 14. Velocity contours with a dimensionless velocity of suction 1 with a suction angle of 90 degrees at 0.1 and 0.25 CHL

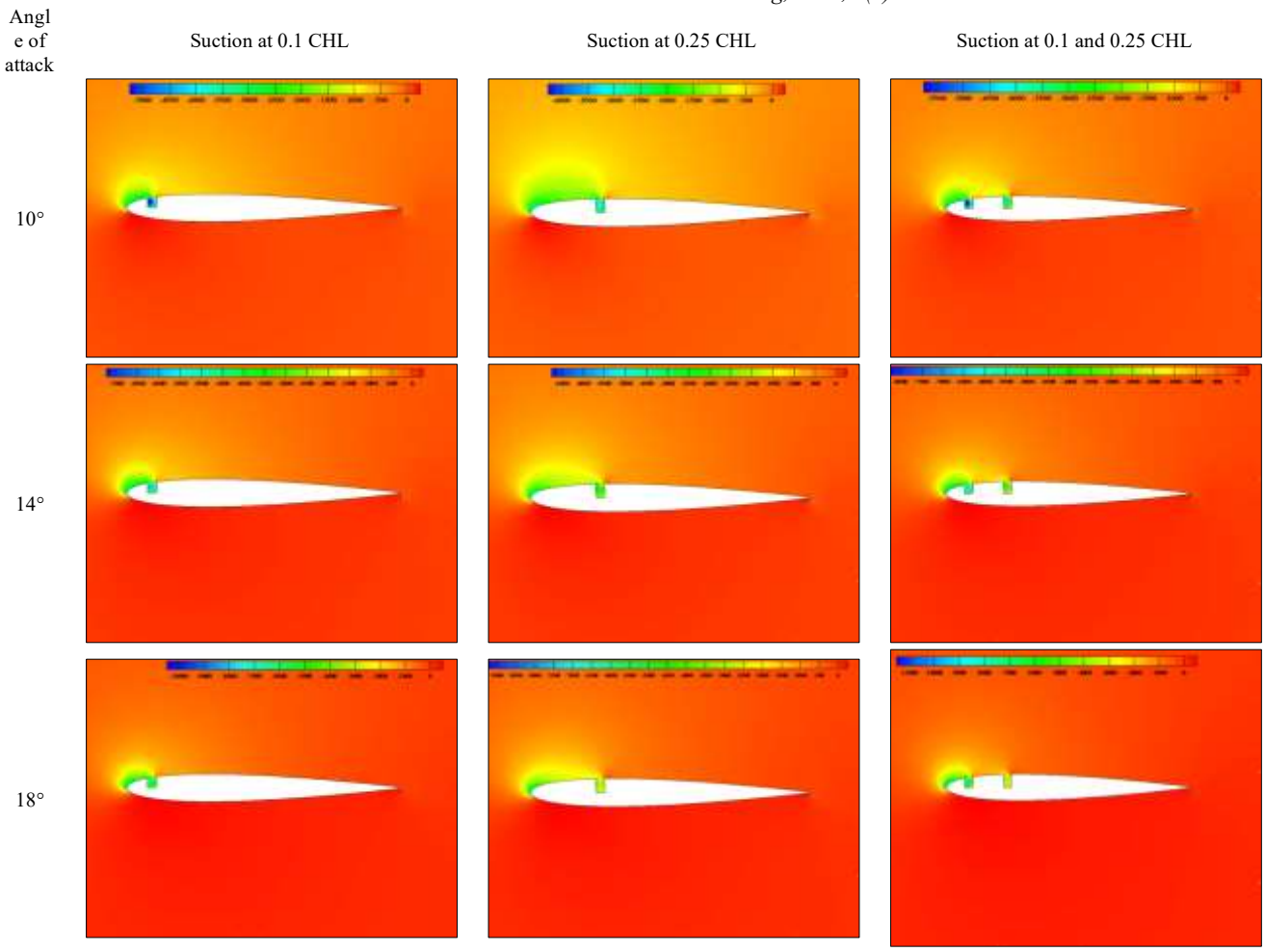

Figure 15. Pressure contours with a dimensionless velocity of suction 1 with a suction angle of 90 degrees at 0.1 and 0.25 CHL

5.2.4.Results in the Dimensionless Velocity of 1

In the analysis of the results of this part according to the pressure contours, at a low angle of attack, such as 10 degrees of suction at 0.1 CHL, a small vortex is observed in the suction gap caused by the movement of the fluid towards the airfoil body. For other angles of attack, this small vortex is not observed. This is because in the initial parts of the airfoil, the thickness of the BL has not yet been formed or is being formed, and the particles from the incoming flow have more energy than the positions where the BL is formed. The high flow velocity causes this small vortex, and the pressure in this area is very low. With the rise of the angle of attack, this small vortex also disappears because the pressure increases.

Regarding the velocity contour, it is obtained that with the rise of the angle of attack, an enormous vortex is formed at the end of the airfoil. As shown in Figure 16, for the position of two suctions, this vortex is smaller than the other two modes, and at the suction position of 0.25, a smaller vortex is formed than at the position of 0.1. Finally, the two-suction mode is the best mode for dimensionless velocity. The diagram of A.Cs is shown in Figure 16 using the numerical values of the C_L and C_D. Tables 3 and 4 show the C_L and C_D values at a suction dimensionless velocity of 1 with a suction angle of 60 and 90 degrees, respectively.

Table 3. C_L and C_D values at a suction dimensionless velocity of 1 with a suction angle of 60 degrees

angle of attack	Suction Angle = 60 Suction position = 0.1 CHL		Suction Angle = 60 Suction position = 0.25 CHL		Suction Angle = 60 Suction position = 0.1 and 0.25 CHL	
	C_L	C_D	C_L	C_D	C_L	C_D
10°	1.4656	-0.00558	1.535522	0.011091	1.495983	-0.04027
12°	1.6559	-0.00233	1.739633	0.018174	1.705329	-0.04355-
14°	1.8232	0.00328	1.9278	0.0288	1.905011	-0.04542
16°	1.954	0.0116	2.0746	0.045208	2.0977	-0.0459
18°	2.015	0.0242	2.1563	0.0655	2.2687	-0.0422

Table 4. C_L and C_D values at a suction dimensionless velocity of 1 with a suction angle of 90 degrees

angle of attack	Suction Angle = 90 Suction position = 0.1 CHL		Suction Angle = 90 Suction position = 0.25 CHL		Suction Angle = 90 Suction position = 0.1 and 0.25 CHL	
	C_L	C_D	C_L	C_D	C_L	C_D
10°	1.456597	-0.01091	1.526327	0.008265	1.479236	-0.04901
12°	1.6533	-0.00983	1.739716	0.015002	1.688787	-0.0541
14°	1.8254	-0.00555	1.9316	0.00251	1.891147	-0.05792
16°	1.971	0.000837	2.0845	0.041305	2.0854	-0.0607
18°	2.06	0.0103	2.1806	0.0614	2.2579	-0.0587

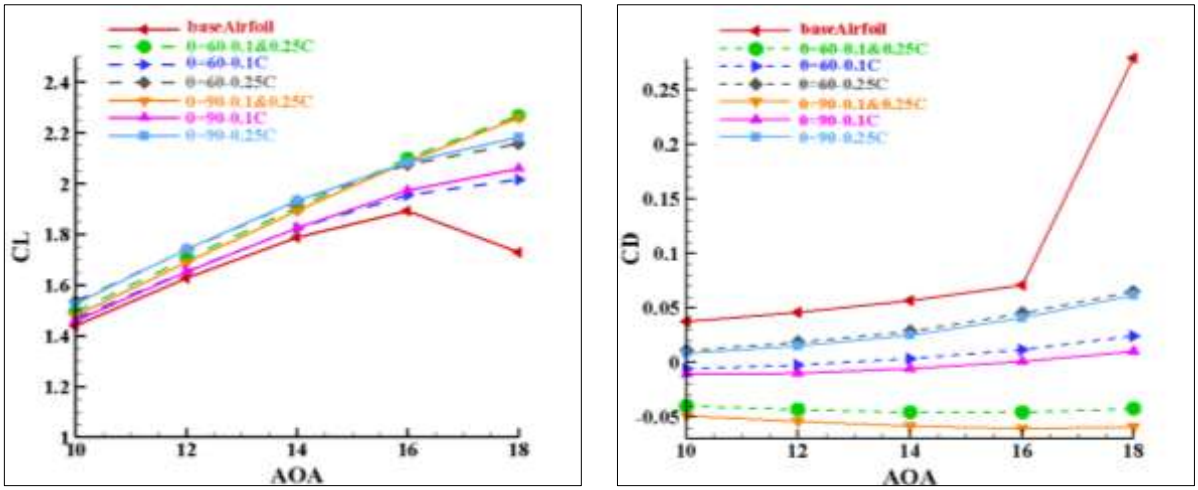

Figure 16. C_L and C_D s at different attack angles at 1 dimensionless velocity

6. Conclusion

In this research, the impacts of suction on the airfoil NACA 0012 were studied and analyzed to control the flow and also determine the optimal length of the suction jet on the upper surface of the airfoil. The effect of changing parameters of suction dimensionless velocity and the suction angle at two positions of 0.1 and 0.25 CHL were numerically modeled, and the subsequent outcomes were achieved.

- Increasing the dimensionless suction velocity increases the C_L, and the separation point moves downstream. The max rise in the C_L was achieved at a dimensionless suction velocity of one and a suction angle of 90 degrees in two suction positions. In this position and at an angle of attack of 18 degrees, the vortices behind the airfoil almost disappeared.
- At low angles of attack, lower than 10 degrees, flow separation control using suction does not significantly increase the aerodynamic properties of the airfoil. However, using suction on the airfoil can improve the stall angle.
- As can be seen in the C_D diagram, for suction at an angle of 90 degrees with a dimensionless velocity of suction 1, a lower C_D is obtained than two suctions with a dimensionless velocity of 0.5, so a suction with a higher velocity can be used here.
- When the number of sections in an airfoil increases, an operator and a suction system are needed, increasing the airfoil's cost and weight. For the C_L, these changes can be seen that almost the same values are obtained for the two modes of a 90-degree suction with a dimensionless velocity of 1 and two suctions with a dimensionless velocity of 0.5, and among these two modes, a suction with a dimensionless velocity of 1 is optimal.

7. References

[1] Ravindran, S. S. (1999). Active control of flow separation over an airfoil (No. NAS 1.15: 209838). National Aeronautics and Space Administration, Washington, United States.

[2] Li, Y., Wang, J., & Zhang, P. (2002). Flow, Turbulence and Combustion, 68(1), 27–39. doi:10.1023/a:1015679408150.

[3] Huang, L., Huang, P. G., LeBeau, R. P., & Hauser, T. (2004). Numerical study of blowing and suction control mechanism on NACA0012 airfoil. Journal of Aircraft, 41(5), 1005–1013. doi:10.2514/1.2255.

[4] You, D., & Moin, P. (2008). Active control of flow separation over an airfoil using synthetic jets. Journal of Fluids and Structures, 24(8), 1349–1357. doi:10.1016/j.jfluidstructs.2008.06.017.

[5] Kim, S. H., & Kim, C. (2009). Separation control on NACA23012 using synthetic jet. Aerospace Science and Technology, 13(4–5), 172–182. doi:10.1016/j.ast.2008.11.001.

[6] Liu, P. Q., Duan, H. S., Chen, J. Z., & He, Y. W. (2010). Numerical study of suction-blowing flow control technology for an airfoil. Journal of Aircraft, 47(1), 229–239. doi:10.2514/1.45114.

[7] Genç, M. S., Kaynak, Ü., & Yapici, H. (2011). Performance of transition model for predicting low Re aerofoil flows without/with single and simultaneous blowing and suction. European Journal of Mechanics, B/Fluids, 30(2), 218–235. doi:10.1016/j.euromechflu.2010.11.001.

[8] Abdullah, T., Laith M. Jasim, D., & Amir S. Dawood, D. (2012). Experimental Study of Lift/Drag Ratio Enhancement Using Continuous Normal Suction. AL-Rafdain Engineering Journal (AREJ), 20(1), 76–84. doi:10.33899/rengj.2012.47159.

[9] Yagiz, B., Kandil, O., & Pehlivanoglu, Y. V. (2012). Drag minimization using active and passive flow control techniques. Aerospace Science and Technology, 17(1), 21–31. doi:10.1016/j.ast.2011.03.003.

[10] Shi, Y., Bai, J., Hua, J., & Yang, T. (2015). Numerical analysis and optimization of boundary layer suction on airfoils. Chinese Journal of Aeronautics, 28(2), 357–367. doi:10.1016/j.cja.2015.02.011.

[11] Zhang, W., Zhang, Z., Chen, Z., & Tang, Q. (2017). Main characteristics of suction control of flow separation of an airfoil at low Reynolds numbers. European Journal of Mechanics - B/Fluids, 65, 88–97. doi:10.1016/j.euromechflu.2017.01.010.

[12] Zhao, Q., Ma, Y., & Zhao, G. (2017). Parametric analyses on dynamic stall control of rotor airfoil via synthetic jet. Chinese Journal of Aeronautics, 30(6), 1818–1834. doi:10.1016/j.cja.2017.08.011.

[13] Ma, D., Li, G., Yang, M., & Wang, S. (2018). Research of the suction flow control on wings at low Reynolds numbers. Proceedings of the Institution of Mechanical Engineers, Part G: Journal of Aerospace Engineering, 232(8), 1515–1528. doi:10.1177/0954410017694057.

[14] Kamari, D., Tadjfar, M., & Madadi, A. (2018). Optimization of SD7003 airfoil performance using TBL and CBL at low Reynolds numbers. Aerospace Science and Technology, 79, 199–211. doi:10.1016/j.ast.2018.05.049.

[15] Kamranpay, A., & Mehrabadi, A. (2019). Numerical Analysis of NACA Airfoil 0012 at Different Attack Angles and Obtaining its Aerodynamic Coefficients. Journal of Mechatronics and Automation, 6(3), 8-16.

[16] Karasu, I., Açikel, H. H., Koca, K., & Genç, M. S. (2020). Effects of thickness and camber ratio on flow characteristics over airfoils. Journal of Thermal Engineering, 6(3), 242–252. doi:10.18186/THERMAL.710967.

[17] Fatahian, E., Lohrasbi Nichkoohi, A., Salarian, H., & Khaleghinia, J. (2020). Effects of the hinge position and suction on flow separation and aerodynamic performance of the NACA 0012 airfoil. Journal of the Brazilian Society of Mechanical Sciences and Engineering, 42(2), 86. doi:10.1007/s40430-020-2170-4.

[18] Akbari, P. (2021). Study of NACA 6212 Airfoil and Investigation of its Aerodynamic Properties in Different Angles of Attack. International Journal of Mechanical Dynamics & Analysis, 7(1), 1–8.

[19] Fatahian, E., & Fatahian, H. (2021). Simultaneous Effect of Suction and Cavity for Controlling Flow Separation on NACA 0012 Airfoil – CFD Approach. Gazi University Journal of Science, 34(1), 235–249. doi:10.35378/gujs.706052.

[20] Kumar, K., Kumar, P., & Singh, S. K. (2021). Passive Control of Boundary Layer Separation Using Single Andmultiple Slats on the Airfoil. International Journal of Fluid Mechanics Research, 48(2), 17–28. doi:10.1615/InterJFluidMechRes.2021033106.

[21] Zhu, Z., Xiao, T., Zhi, H., Deng, S., & Lu, Y. (2022). Aerodynamic characteristics of co-flow jet wing with simple high-lift devices. Chinese Journal of Aeronautics, 35(10), 67–83. https://doi.org/10.1016/j.cja.2022.03.008.

[22] Açıkel, H. H., Tosun, M., Genç, M. S., & Koca, K. (2022). Numerical investigation on NACA0012 airfoil with tubercular structure. EPJ Web of Conferences, 269, 01001. doi:10.1051/epjconf/202226901001.

[23] Mishra, A., & De, A. (2023). Investigation of Flow Over Naca0021 Airfoil With Leading-Edge Tubercles Using Transition-Based Hybrid Rans/Les Model. Journal of Flow Visualization and Image Processing, 30(1), 1–36. doi:10.1615/JFlowVisImageProc.2022040289.

[24] Ma, C. Y., Xu, H. Y., & Qiao, C. L. (2023). Comparative study of two combined blowing and suction flow control methods on pitching airfoils. Physics of Fluids, 35(3). doi:10.1063/5.0138962.

[25] Rayhan, A. M., Hossain, M. S., Mim, R. H., & Ali, M. (2024). Computational and experimental study on the aerodynamic performance of NACA 4412 airfoil with slot and groove. Heliyon, 10(11). doi:10.1016/j.heliyon.2024.e31595.

[26] Butt, F., Talha, T., Khan, R., Mazhar, A. R., Butt, M., Petru, J., & Seikh, A. H. (2024). Effect of the shape of flapping airfoils on aerodynamic forces. Heliyon, 10(8). doi:10.1016/j.heliyon.2024.e29561.

[27] Abdalkarem, A. A. M., Ansaf, R., Muzammil, W. K., Ibrahim, A., Harun, Z., & Fazlizan, A. (2023). Preliminary assessment of the NACA0021 trailing edge wedge for wind turbine application. Heliyon, 9(11). doi:10.1016/j.heliyon.2023.e21193.

[28] Khalili, Z., Bararpour, A., Hosseinzadeh, K., Jafari, B., & Domiri Ganji, D. (2024). New Approach of Non-Linear Fractional Differential Equations Analytical Solution by Akbari-Ganji's Method. Contributions of Science and Technology for Engineering, 1(1), 13–19.

[29] Krishnaswamy, S., Jain, S., & Sitaram, N. (2014). Grid and Turbulence Model-based Exhaustive Analysis of NACA 0012 Airfoil. Journal of Advanced Research in Applied Mechanics & Computational Fluid Dynamics, 1(1), 24–33.